Response to reviewers' comments on "Elucidation of the myrcene ozonolysis mechanism from a Criegee Chemistry perspective"

Response to Reviewer #2

This manuscript presents a comprehensive investigation of myrcene ozonolysis from the perspective of Criegee intermediate (CI) chemistry. Using a combination of MI-FTIR, smog-chamber experiments, UHPLC-Orbitrap MS, and quantum chemical calculations, the authors identify both C3-CIs and C7-CIs, and evaluate their distinct contributions to secondary organic aerosol (SOA) formation. The work proposes a potentially important synergistic mechanism between SCIs oligomerization and RO_2 autoxidation, offering new insights into particle nucleation in monoterpene systems.

Thank you for giving us the opportunity to revise our manuscript. We appreciate reviewer for your time and constructive comments, which have helped us significantly improve the quality of our work. We have carefully considered all points raised and have made extensive revisions to the manuscript accordingly. Below, we provide a point-by-point response to each comment. Our detailed responses are provided below (in blue). The manuscript has been thoroughly revised accordingly (in red), with all changes highlighted in *italics*, including new analyses added to address the specific comments.

Major issues:

1. Criegee intermediates are produced in the ozonolysis of myrcene as proposed in Figure 1. It is noted that the formed Criegee intermediates contain C=C group and COO group, which could lead to the C=C group reaction with COO group similar to the previous investigation in the literature (Nat. Commun. 2019, 10, 2003.).

The author's answer: Thank you for your comments. We are grateful for your highly innovative suggestion. Indeed, we were aware of this literature (Nat. Commun. 2019, 10, 2003) at the inception of our study. As shown in Figure R1(1), the unimolecular degradation pathways of CIs with a C=O group from the literature were provided. It was plausible that this pathway was accessible to C7-CIs, as shown in Figure R1(2). However, after a detailed examination of the structural features of the C7-CIs, we concluded that the mechanism reported in the literature did not represent the dominant pathway for the unimolecular degradation of the C7-CIs produced in myrcene ozonolysis. A detailed explanation was provided below.

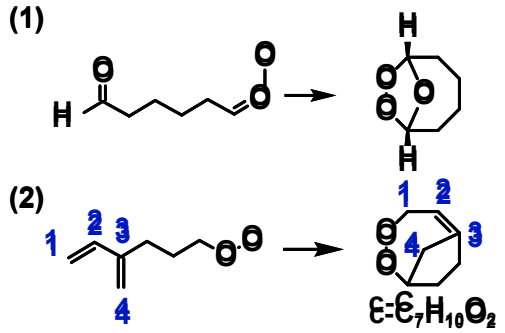

Figure R1 The unimolecular decomposition of CIs.

(1) The C=C group of the C7-CIs was part of a conjugated system, which conferred significant stability and resists being broken.

(2) Weak interaction analysis based on the interaction region indicator (IRI) method was conducted for the most stable configuration of C7-CIs as shown in Figure R2 (Lu and Chen, 2021). The blue, green, and red colors in Figure R2 represented the bond interactions, Van der Waals interactions, and steric effects, respectively. The results indicated no interaction between the terminal -COO group and the C=C moiety (Figure R2(a) and (b)). In contrast, weak interactions were identified between the -COO group and the β- and γ-H atoms (Figure R2(a)), implying a potential preference of syn-C7-CIs for unimolecular degradation through an H-transfer mechanism. Analysis of anti-C7-CIs reveals that no weak interactions were present between the -COO group and the C=C moiety (Figure R2(b)). Structurally, the simultaneous addition of the -COO group to C1 and C4 in C7-CIs required considerable molecular distortion, suggesting a potentially high energy barrier for this pathway.

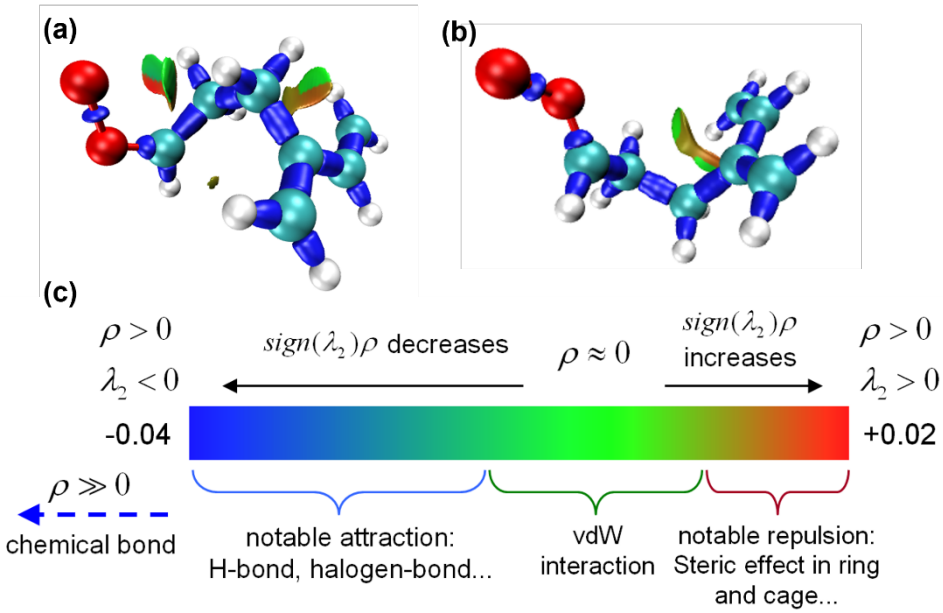

Figure R2 The isosurface maps of syn-C7-CIs (a) and anti-C7-CIs (b) were obtained via the IRI method. Standard coloring method and chemical explanation of *sign*(λ_2)ρ on IRI isosurfaces (c).

(3) Considering the new unimolecular pathway noted by the reviewer, the resulting product c-$C_7H_{10}O_2$, which contained a double bond, could react further to form $C_7H_{12}O_5$ and $C_7H_{10}O_4$ as potential

subsequent products (Figure R3). In the absence of a scavenger, the mass spectral intensities for $C_7H_{12}O_5$ (m/z 177.076) and $C_7H_{10}O_4$ (m/z 159.065) were 4% and 10%, respectively. Both compounds were minor constituents in particle. And this degradation pathway did not generate RO_2 radicals or the corresponding $C_7H_{10}O_X$ (X=2-5) products. Our analysis revealed the presence of $C_7H_{10}O_X$ (X=2-5) products, as shown in Figure 5 of the manuscript. Therefore, we determined it was not a major degradation (Nat. Commun. 2019, 10, 2003) route for C7-CIs.

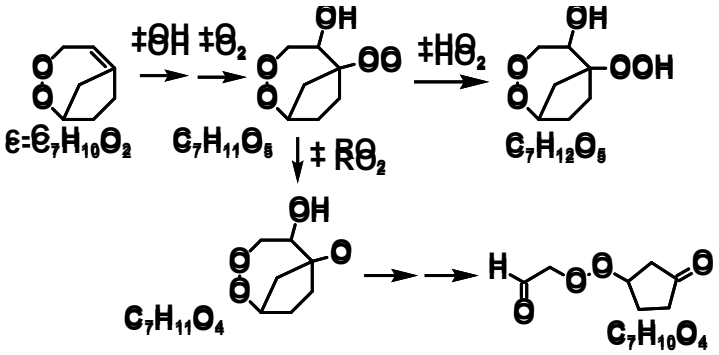

Figure R3 The reaction pathway of $C_7H_{10}O_2$.

Lines 39, we added this references to "*Compared to anti-CIs, syn-CIs are more prone to undergo unimolecular degradation reactions (Long et al., 2018, **2019**; Vereecken et al., 2017).*".

In the References part, **lines 483-484**, we added "*Long, B., Bao, J. L., and Truhlar, D. G.: Rapid unimolecular reaction of stabilized Criegee intermediates and implications for atmospheric chemistry, Nat. Commun., 10, 2003, 10.1038/s41467-019-09948-7, 2019.*".

2. Although I think that the calculated results can be used to help explain the experimental measurements, it is better to explain the error bars due to the computational methods. This is very helpful for potential readers to understand the challenges in the calculations.

The author's answer: Thank you for your comments. As the reviewer noted, discrepancies could exist between calculated and experimental values for infrared spectra. Calculational levels commonly were employed to calculate POZs and CIs in VOCs ozonolysis systems include: B3LYP-D3(BJ)/6−311++G(d,p) (Yu et al., 2025), B3LYP-D3(BJ)/aug-cc-pVTZ (Lv et al., 2017), B3LYP/6-311G++(d,2p) (Hoops and Ault, 2009; Coleman and Ault, 2010, 2013; Pinelo et al., 2013), B3LYP/6-311++G(2d,2p) (Yang et al., 2020; Deng et al., 2012). To address the discrepancies among the computational methods, we calculated the infrared spectra of carbonyl oxides (CIs) containing 1 to 3

carbon atoms as well as those with 7 carbon atoms mentioned in the manuscripts using the method described above.

Table R1 The characteristic infrared peaks of CIs were obtained using different computational methods.

CIs	Calculated band/(cm^{-1})				**Experimental band/ (cm^{-1}) [a]**	Assignment
	B3LYP-D3(BJ)/ 6−311++G(d,p)	B3LYP-D3(BJ)/ aug-cc-pVTZ	**B3LYP/6-311G++(d,2p)**	B3LYP/ 6-311++G(2d,2p)		
Anti-CH_3CHOO	961	968	**961**	971	**884**	O-O stretch
Syn-CH_3CHOO	884	897	**882**	908.17	**871.2**	O-O stretch
$(CH_3)_2COO$	912	925	**909**	928	**887.4**	O-O stretch
CH_2OO	899	912	**901**	923	**909**	O-O stretch
Syn-C7-CIs	883	893	**882**	900	\	O-O stretch
Anti-C7-CIs	912	923	**910**	928	\	O-O stretch

Note: [a] Data from references (Chhantyal-Pun et al., 2020a).

As shown in Table R1, the table correspondingly list only the peak positions associated with this vibration because of the manuscript focused solely on the most intense O-O stretching vibration of CIs. Among the four computational methods, the B3LYP/6-311G++(d,2p) level demonstrated superior performance in predicting the O-O stretching vibrational frequencies of CIs. The results from this method were also in close agreement with the computational values reported previously by Li et al (Lin et al., 2015; Su et al., 2013; Wang et al., 2016). Thus, we have recalculated the infrared spectra of all relevant configurations in our manuscript using the B3LYP/6-311G++(d,2p) method and incorporated the necessary revisions. It could be observed that the calculated peak positions for alkyl-substituted CIs were systematically overestimated compared to the available experimental values. For example, a significant discrepancy of 77 cm^{-1} was noted for anti-CH_3CHOO. In contrast, the deviation was much smaller for syn-CH_3CHOO being only 10.8 cm^{-1}. This was consistent with the trend previously observed by Li et al (Lin et al., 2015). Therefore, the computational results provided strong support for the identification of syn-C7-CIs.

Due to the discrepancies between the calculated and experimental infrared spectra, the computational results were not the sole basis for our peak assignments. For example, we observed that POZs and CIs appear sequentially. The characteristic peaks of POZs emerged first at lower temperatures. As the temperature increased, the infrared signals of CIs, along with those of the concurrently formed aldehydes, then became detectable. In addition, the characteristic IR peak ranged for CIs and POZs have been summarized from the literature, thereby providing a key basis for our spectral assignments.

Lines 14, we changed “Two CIs with different molecular sizes, C3-CIs and C7-CIs, are captured at 880

and 905 cm^{-1} by using MI-FTIR." to "*C3-CIs are captured at 880 cm^{-1} by using MI-FTIR.*".

Lines 136-139, we modified "The geometries of the SCIs were optimized using the hybrid density functional theory B3LYP-D3(BJ) with the aug-cc-pVTZ basis set. Harmonic vibrational frequencies were calculated at B3LYP/6-311G++(d,2p) calculation level for the comparison with the experimental infrared peak. Various computational levels for CIs were compared, and the one with superior performance was selected accordingly. Please refer to Table S1 for the specific comparison." to "*The geometries of the myrcene, POZs and SCIs were optimized using the hybrid density functional theory B3LYP-D3(BJ) with the aug-cc-pVTZ basis set. Harmonic vibrational frequencies were calculated at B3LYP/6-311G++(d,2p) calculation level for the comparison with the experimental infrared peak. Various computational levels for CIs were compared, and the one with superior performance was selected accordingly. Please refer to Table S1 for the specific comparison.*".

Correspondingly, Table R1 has been added to the supporting information (Table S1). The following explanation was added beneath the Table S1: "*As shown in Table R1, the table correspondingly list only the peak positions associated with this vibration because of the manuscript focused solely on the most intense O-O stretching vibration of CIs. Among the four computational methods, the B3LYP/6-311G++(d,2p) level demonstrated superior performance in predicting the O-O stretching vibrational frequencies of CIs. The results from this method were also in close agreement with the computational values reported previously by Li et al (Lin et al., 2015; Su et al., 2013; Wang et al., 2016). Thus, we have recalculated the infrared spectra of all relevant configurations in our manuscript using the B3LYP/6-311G++(d,2p) method and incorporated the necessary revisions. It could be observed that the calculated peak positions for alkyl-substituted CIs were systematically overestimated compared to the available experimental values. For example, a significant discrepancy of 77 cm^{-1} was noted for anti-CH_3CHOO. In contrast, the deviation was much smaller for syn-CH_3CHOO being only 10.8 cm^{-1}. This was consistent with the trend previously observed by Li et al (Lin et al., 2015). Therefore, the computational results provided strong support for the identification of syn-C7-CIs.*".

Lines 187-192, we modified "The calculated O-O stretching vibrations of C7-CIs were located at 892 (syn-C7-CIs) and 923 (anti-C7-CIs) cm^{-1}, which were covered by the main characteristic infrared vibration peaks of myrcene. Consequently, it was challenging to directly observe the strongest characteristic infrared vibration peaks belonging to C7-CIs. In addition to the -COO group, C7-CIs also possessed conjugated double bonds as characteristic functional groups. In both syn- and anti-C7-CIs, the

second most intense infrared vibration band consistently corresponded to the wagging vibration of the $=CH_2$ group on the conjugated moiety. The calculated position of this vibration agreed with that of myrcene. Position 905 cm^{-1} was the infrared characteristic peak generated by the wagging vibration of myrcene $=CH_2$, as obtained by twin-jet method. In the spectra, a significant relative increase at the 905 cm^{-1} position was observed after annealing to 55 K. This increase might be attributable to the generation of C7-CIs. The characteristic infrared peaks of C3- and C7-CIs were both generated after 55 K annealing." to "*The calculated O-O stretching vibrations of C7-CIs were located at 882 (syn-C7-CIs) and 910 (anti-C7-CIs) cm^{-1}. According to Table S1, the calculated IR peaks of CIs were consistently overestimated by over 10 cm^{-1} relative to experimental values, with the deviation being most pronounced for anti-CIs. Notably, no distinct new peaks appeared below 882 cm^{-1} in the experiment. This absence suggested that very few stabilized C7-CIs were likely generated during the ozonolysis of myrcene. Instead, most C7-CIs were consumed via unimolecular decay pathways, a conclusion which was also supported by our subsequent analysis.*".

Lines 178-179, we modified "The calculation results indicated that the C-O stretching vibrations of the two POZs were located at positions 1068 and 1174 cm^{-1}." to "*The calculation results indicated that the C-O stretching vibrations of the two POZs were located at positions 1059 and 1165 cm^{-1}.*".

Lines 202, the Table 1 was changed as shown below.

Table 1 Identification and assignments of experimental absorption bands in the initial ozonolysis of myrcene.

Experimental bands/(cm^{-1})	*Calculated Band/(cm^{-1})*	*Reference*	*Belonger*	*Assignment*
765	\	*772*	*POZs*	*O-O-O str.*
880	\	*887* [a]	*C3-CIs*	*O-O str.*
905			*4-vinyl-4-pentenal*	*$=CH_2$ wag.*
1074	*1054*	\	*POZs*	*C-O str.*
1177	*1165*	\	*POZs*	*C-O str.*
1370	\	*1370* [b]	*Acetone*	*δ CH_3*
1720	\	*1721.6* [b]	*Acetone*	*C=O str.*

Lines 345-348, in the Conclusion part, we changed "This study employed the MI-FTIR method to directly determine the presence of C3-CIs and C7-CIs during the myrcene ozonolysis. The characteristic infrared vibration peak of C7-CIs, caused by the $=CH_2$ wagging vibration on the conjugated double bonds, was located at 905 cm^{-1}." to "*This study employed the MI-FTIR method to determine the presence of C3-CIs*

and C7-CIs during the myrcene ozonolysis. The O-O stretching vibration peak of C3-CIs was located at 880 cm^{-1}. The absence of characteristic infrared peaks belonged to C7-CIs, likely due to their low steady-state yield or rapid unimolecular decay. The characteristic IR peaks of acetone indirectly confirmed the production of C7-CIs.".

Minor issues

1. Figure 1: Make the font of this figure consistent with those of the other figures in the entire text.

The author's answer: Thank you for your comments. We have modified Figure 1. The revised Figure 1 was as follows:

Lines 161,

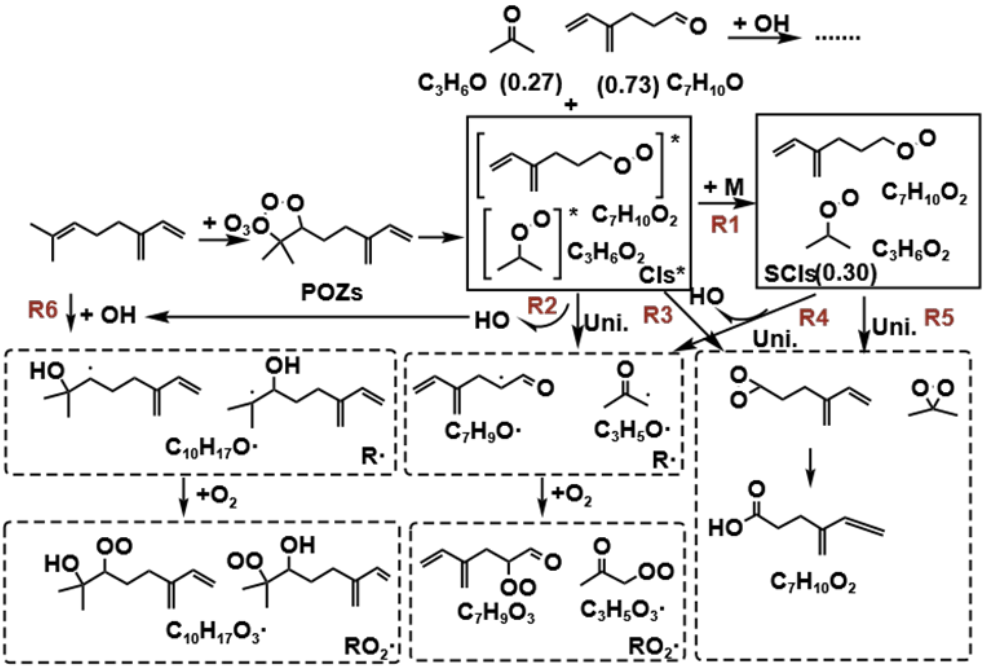

Figure 1 Proposed the key pathway in the initial ozonolysis of myrcene. The values in parentheses represent the yields of the corresponding products.

2. Figure 2: How to confirm that the 905 cm^{-1} peak is the characteristic IR peak for C7-CIs, given the overlap with the parent peak and the presence of other products with conjugated double bonds, such as POZ.

The author's answer: Thank you for your comments. First, the spectra of a single precursor (myrcene/Ar or O_3/Ar) were conducted at different temperatures. The results showed that temperature variation did not alter the intensity of the infrared characteristic peak of myrcene or O_3 at 905 cm^{-1} as shown in Figure S1(a). Based on a re-examination of the characteristic IR peaks of C7-CIs, we concluded that no such

peaks were observed in our experiments. However, in the spectrum from the twin-jet experiment at 55 K, the relative peak intensity at this wavenumber increased significantly. This indicated the formation of new species exhibiting a characteristic vibration at this location. The characteristic IR bands of C3-CIs could only be detected at 55 K, and the intensity change of the peak at 905 cm^{-1} followed this consistent behavior. Therefore, the 905 cm^{-1} position might be attributed to the 4-vinyl-4-pentenal (C7-aldehyde) which also contained conjugated double bonds.

The characteristic IR peaks at 892 and 905 cm^{-1} for myrcene were due to the wagging vibrations of the $=CH_2$ groups terminating its conjugated diene system. The characteristic IR peaks for POZs emerged at a lower temperature (35 K) compared to CIs (55 K). Within the 35-45 K range, the peak at 892 cm^{-1} remained more intense than that at 905 cm^{-1} (Figure R4), suggesting the former was more likely due to the $=CH_2$ wagging of POZs. Consequently, the 905 cm^{-1} feature was assigned to C7- aldehyde based on its distinct temperature-dependent behavior.

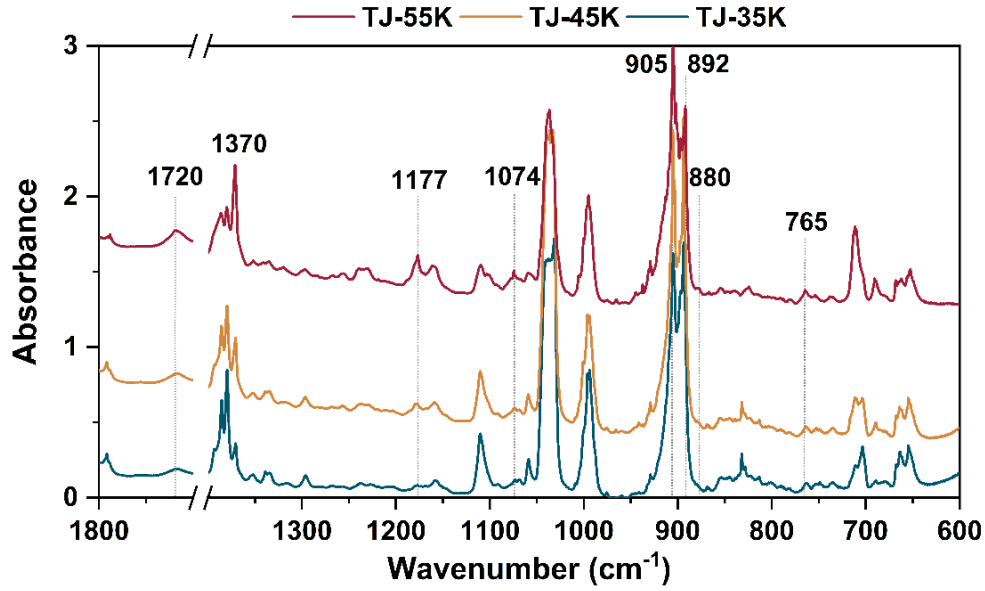

Figure R4 The twin-jet spectra of myrcene ozonolysis reaction in a low temperature and Ar matrix after annealing to 35 K, 45 K and 55 K. T-J means the spectra obtained by twin-jet method.

Lines 148-149, we changed "The products generated along with C7-CIs and C3-CIs were acetone and 4-vinyl-4-pentental with yields of 0.27 and 0.73, respectively." to "*The products generated along with C7-CIs and C3-CIs were acetone and 4-vinyl-4-pentental (C7-aldehyde) with yields of 0.27 and 0.73, respectively.*".

Lines 195-196, we added "*The peak at 905 cm^{-1} coincided in temperature with the C3-CIs peaks and suggested its assignment to the $=CH_2$ wagging vibration of the C7-aldehyde.*".

3. Regarding the matrix isolation experiment, what are the scientific considerations governing the choice of the specific temperature window, namely 35-55 K?

The author's answer: Thank you for your comments. For traditional matrix isolation experiments that used the inert gas argon as the matrix, the commonly used temperature range was ≤ 35 K. In our myrcene ozonolysis experiment, we advanced beyond the conventional matrix isolation scheme. By elevating the matrix temperature, the precursors overcame the confinement of the matrix "cage". This allowed the precursors to make more sufficient contact and react more thoroughly, thereby leading to a significant enhancement of the infrared characteristic peaks of the intermediates and products. However, gradual heating under the high vacuum conditions of matrix isolation led to precursor loss, prompting us to cap the maximum temperature at 55 K.

This approach was echoed by existing studies. For instance, Yu et al., while investigating the ozonolysis of styrene using the same methodology, employed a temperature range of 6 K to 57 K. They observed the most intense characteristic peaks of the intermediates and products precisely at 57 K (Yu et al., 2025). In studying the ozonolysis mechanism of tetramethylethylene, Yang et al. adopted a higher experimental temperature to detect final products (Yang et al., 2020).

Lines 107, in the 2.1 Matrix isolation experiment part, we cited the two above-mentioned references in the following sentence, "*To promote the further occurrence of the reaction and further soften and diffuse the matrix, the matrix was further heated to 45 and 55 K (Yu et al., 2025; Yang et al., 2020).*".

4. Section 3.2, How to confirm that SCIs first react with RO_2 and then with HO_2, rather than RO_2 first reacting with HO_2 to form ROOH, which then reacts with SCIs.

The author's answer: Thank you for your comments. Current evidence showed that the reaction between SCIs and RO_2 was considerably faster than that between SCIs and ROOH. Zhao et al. used quantum chemical calculations to compare the free energy barriers and found that the formation of ROO-SCIs-H prefers to follow the RO_2 + SCIs + HO_2 reaction rather than the ROOH + SCIs reaction (Zhao et al., 2017). The reaction rate between CH_2OO and CH_3O_2 was determined by UV-vis spectroscopy to be $(1.7 \pm 0.5)\times10^{-11}$ cm^3 s^{-1} at 294 K and 10 Torr (Chao et al., 2024). Chhantyal-Pun et al. measured the reaction rate of CH_2OO with CH_3O_2/$CH_3C(O)O_2$ using cavity ring-down spectroscopy, obtaining a value of $(2.4 \pm 1.2)\times10^{-11}$ cm^3 $molecule^{-1}$ s^{-1} (Chhantyal-Pun et al., 2020b). However, the reaction rates of CH_2OO with

H_2O_2 and $(CH_3)_3COOH$ (peroxides) were determined to be $(2.2\pm0.9) \times 10^{-13}$ and $(1.2^{+1.2}_{-0.6}) \times 10^{-13}$ cm^3 $molecule^{-1}$ s^{-1}, respectively (Caravan et al., 2024). And existing studies indicated that oligomers were produced via the RO_2 + SCIs + HO_2 mechanism, as opposed to the RO_2 + HO_2 + SCIs mechanism (Yu et al., 2025; Zhao et al., 2015). Therefore, we concluded that the predominant formation pathway for oligomers proceeded via RO_2 + SCIs + HO_2 rather than RO_2 + HO_2 + SCIs.

Lines 258-260, we added "*The rate constants for the reaction of RO_2 radicals with SCIs were much higher than that for ROOH (Zhao et al., 2017; Chao et al., 2024; Chhantyal-Pun et al., 2020; Caravan et al., 2024).*".

5. The authors characterized the particulate phase composition and detected oligomers within it. How can it be demonstrated that these oligomers were formed in the gas phase rather than in the particle phase? For instance, oligomers can also be formed by hemiacetal reactions within the particle phase. How is this particle-phase pathway accounted for?

The author's answer: Thank you for your comments. The rate constant for reactions between CIs and organic acids approached the collision limit, approximately 10^{-10} cm^3 $molecule^{-1}$ s^{-1}, while the rate constant for reactions with RO_2 radicals was on the order of 10^{-11} cm^3 $molecule^{-1}$ s^{-1}. These exceptionally high gas-phase rate constants resulted in the near-complete consumption of CIs in the gas phase, leading to their conversion into less volatile products that subsequently partition into the particle phase. Several studies have identified CIs oligomerization as a contributor to particle formation, and categorizing this reaction pathway as a gas-phase process (Yu et al., 2025; Zhao et al., 2015; Caravan et al., 2024). The mass spectral signals of the oligomers exhibited an enhancing trend following the introduction of the OH scavenger. This demonstrated that the oligomers predominantly originated from CIs-derived channels.

A substantial contribution from the hemiacetal reaction to the particle phase typically necessitated an acid-catalyzed system, involving the introduction of acids (Zhao et al., 2015). As this was not the case in our study, the oligomers were consequently not attributed to acid catalysis.

6. Equation R8 contains an error in its chemical formula.

The author's answer: Thank you for your comments. We have modified Formula R8. The revised R8 is as follows.

Lines 291,

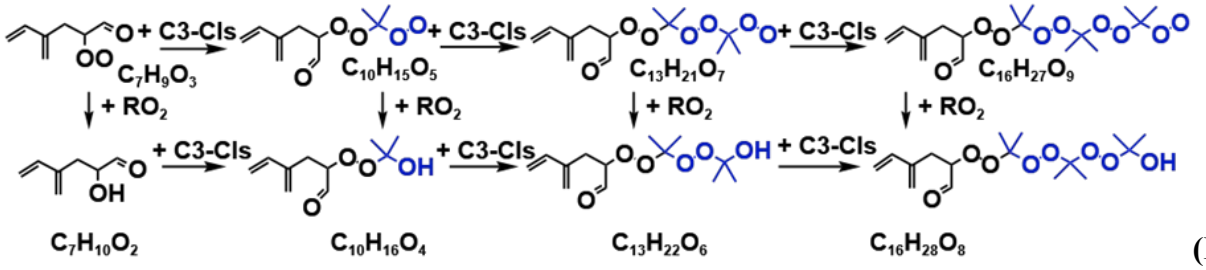

(R8)

References

Caravan, R. L., Bannan, T. J., Winiberg, F. A. F., Khan, M. A. H., Rousso, A. C., Jasper, A. W., Worrall, S. D., Bacak, A., Artaxo, P., Brito, J., Priestley, M., Allan, J. D., Coe, H., Ju, Y., Osborn, D. L., Hansen, N., Klippenstein, S. J., Shallcross, D. E., Taatjes, C. A., and Percival, C. J.: Observational evidence for Criegee intermediate oligomerization reactions relevant to aerosol formation in the troposphere, Nat. Geosci., 17, 219–226, 10.1038/s41561-023-01361-6, 2024.

Chao, W., Markus, C. R., Okumura, M., Winiberg, F. A. F., and Percival, C. J.: Chemical Kinetic Study of the Reaction of CH_2OO with CH_3O_2, J. Phys. Chem. Lett., 15, 3690-3697, 10.1021/acs.jpclett.4c00159, 2024.

Chhantyal-Pun, R., Khan, M. A. H., Taatjes, C. A., Percival, C. J., Orr-Ewing, A. J., and Shallcross, D. E.: Criegee intermediates: production, detection and reactivity, Int. Rev. Phys. Chem., 39, 383-422, 10.1080/0144235x.2020.1792104, 2020a.

Chhantyal-Pun, R., Khan, M. A. H., Zachhuber, N., Percival, C. J., Shallcross, D. E., and Orr-Ewing, A. J.: Impact of Criegee Intermediate Reactions with Peroxy Radicals on Tropospheric Organic Aerosol, Acs Earth Space Chem., 4, 1743-1755, 10.1021/acsearthspacechem.0c00147, 2020b.

Coleman, B. E. and Ault, B. S.: Matrix isolation investigation of the ozonolysis of propene, J. Mol. Struct., 976, 249-254, https://doi.org/10.1016/j.molstruc.2010.03.050, 2010.

Coleman, B. E. and Ault, B. S.: Investigation of the mechanism of ozonolysis of (Z)-3-methyl-2-pentene using matrix isolation infrared spectroscopy, J. Mol. Struct., 1031, 138-143, https://doi.org/10.1016/j.molstruc.2012.07.046, 2013.

Deng, J., Chen, J., Liu, H., Wang, W., and Wang, X.: Matrix Isolation FT-IR Study on the Reaction Mechanisms between Ozone and Ethene, Res. Environ. Sci., 25, 1-9, 2012.

Hoops, M. D. and Ault, B. S.: Matrix Isolation Study of the Early Intermediates in the Ozonolysis of Cyclopentene and Cyclopentadiene: Observation of Two Criegee Intermediates, J. Am. Chem. Soc., 131, 2853-2863, 10.1021/ja8065286, 2009.

Lin, H.-Y., Huang, Y.-H., Wang, X., Bowman, J. M., Nishimura, Y., Witek, H. A., and Lee, Y.-P.: Infrared identification of the Criegee intermediates syn- and anti-CH_3CHOO, and their distinct conformation-dependent reactivity, Nat. Commun., 6, 7012, 10.1038/ncomms8012, 2015.

Lu, T. and Chen, Q.: Interaction Region Indicator: A Simple Real Space Function Clearly Revealing Both Chemical Bonds and Weak Interactions, Chem. Method, 1, 231-239, 10.1002/cmtd.202100007, 2021.

Lv, C., Du, L., Tang, S. S., Tsona, N. T., Liu, S. J., Zhao, H. L., and Wang, W. X.: Matrix isolation study of the early intermediates in the ozonolysis of selected vinyl ethers, Rsc Adv., 7, 19162-19168, 10.1039/c7ra01011g, 2017.

Pinelo, L., Gudmundsdottir, A. D., and Ault, B. S.: Matrix Isolation Study of the Ozonolysis of 1,3-and 1,4-Cyclohexadiene: Identification of Novel Reaction Pathways, J. Phys. Chem. A, 117, 4174-4182, 10.1021/jp402981n, 2013.

Su, Y.-T., Huang, Y.-H., Witek, H. A., and Lee, Y.-P.: Infrared Absorption Spectrum of the Simplest Criegee Intermediate CH_2OO, Science, 340, 174-176, 10.1126/science.1234369, 2013.

Wang, Y.-Y., Chung, C.-Y., and Lee, Y.-P.: Infrared spectral identification of the Criegee intermediate $(CH_3)_2COO$, J. Chem. Phys., 145, 154303, 10.1063/1.4964658, 2016.

Yang, X., Deng, J., Li, D., Chen, J., Xu, Y., Zhang, K., Shang, X., and Cao, Q.: Transient species in the ozonolysis of tetramethylethene, J. Environ. Sci., 95, 210-216, 10.1016/j.jes.2020.03.027, 2020.

Yu, S. S., Tong, S. R., Chen, M. F., Zhang, H. L., Xu, Y. Y., Guo, Y. C., and Ge, M. F.: Characterization of Key Intermediates and Products from the Ozonolysis of Styrene-Like Compounds, Environ. Sci. Technol., 10.1021/acs.est.5c00769, 2025.

Zhao, Q., Wang, W., Liu, F., Lu, J., and Wang, W.: Oligomerization reactions for precursors to secondary organic aerosol:

Comparison between two formation mechanisms for the oligomeric hydroxyalkyl hydroperoxides, Atmos. Environ., 166, 1-8, 10.1016/j.atmosenv.2017.07.008, 2017.

Zhao, Y., Wingen, L. M., Perraud, V., Greaves, J., and Finlayson-Pitts, B. J.: Role of the reaction of stabilized Criegee intermediates with peroxy radicals in particle formation and growth in air, Phys. Chem. Chem. Phys., 17, 12500-12514, 10.1039/c5cp01171j, 2015.